ACS Catalysis

Research Article

pubs.acs.org/acscatalysis

Highly Active MnN–Li_2NH Composite Catalyst for Producing CO_x-Free Hydrogen

Jianping Guo,[†,‡] Fei Chang,[†,‡] Peikun Wang,[†,‡] Daqiang Hu,[†,∥] Pei Yu,[†,‡] Guotao Wu,[†] Zhitao Xiong,[†] and Ping Chen*[,†,§]

[†]Dalian Institute of Chemical Physics, Chinese Academy of Sciences, Dalian 116023, People's Republic of China

[‡]University of Chinese Academy of Sciences, Beijing 100049, People's Republic of China

[§]State Key Laboratory of Catalysis, Dalian Institute of Chemical Physics, Chinese Academy of Sciences, Dalian 116023, People's Republic of China

Supporting Information

ABSTRACT: We report on the significant synergistic effect of Li_2NH on MnN in catalyzing NH_3 decomposition to produce CO_x-free hydrogen. The MnN–Li_2NH exhibits catalytic activity below 623 K and reaches a hydrogen production rate of 37.5 $mmol_{H_2}\ g_{cat}^{-1}\ min^{-1}$ at 773 K, which is ~40 times the MnN and even superior to the highly active Ru-based catalysts under the same conditions. The apparent activation energy of MnN–Li_2NH is similar to that of Ru/CNTs. The stability of the MnN–Li_2NH composite catalyst depends on the molar ratio of MnN and Li_2NH, and the catalyst with higher Mn content shows better stability. Our experimental results reveal that Li_2NH reacts with MnN, giving rise to H_2 and Li_7MnN_4; Li_7MnN_4, on the other hand, can be easily ammoniated to give off N_2, which suggests that the catalysis is fulfilled via a redox cycle comprising (I) $Li_2NH + MnN \rightarrow Li_7MnN_4 + H_2$ and (II) $Li_7MnN_4 + NH_3 \rightarrow MnN + Li_2NH + N_2$. The presence of Li_2NH favors the formation of N-rich intermediate Li_7MnN_4, where Li^+ executes a positive inductive effect to enhance the covalent Mn–N bonding and, therefore, leads to an altered reaction pathway and energetics. Our kinetic analyses indicate that the H_2 release step encounters a relatively higher barrier than the N_2 release step.

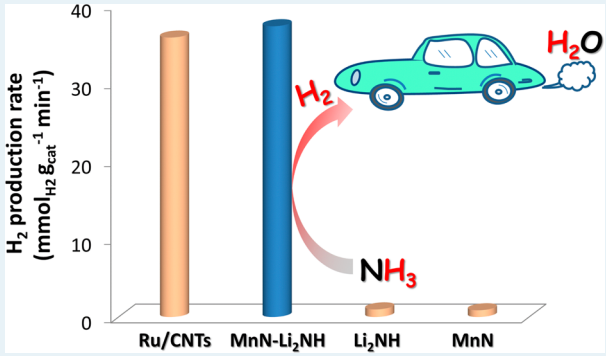

KEYWORDS: *manganese nitride, lithium imide, ternary lithium nitride, ammonia decomposition, heterogeneous catalysis*

1. INTRODUCTION

With a high hydrogen content (17.7 wt %), high energy density (4 kWh kg^{-1}), and facile storage and transportation, NH_3 has been regarded as a potential CO_x-free hydrogen carrier.[1−3] Achieving a high NH_3 conversion rate at relatively low temperatures remains challenging, albeit ~99% conversion is thermodynamically allowed at 673 K as a result of the mild endothermic nature of the reaction. To date, a variety of transition metals, alloys, carbides, and nitrides have been found to be catalytically active to NH_3 decomposition reaction,[1,4−11] among which Ru-based catalysts, especially those supported on CNTs[1,12] and inorganic electride,[13] appear to be the most active. However, the high price and limited supply of Ru hinders its practical applications. The development of a nonnoble metal catalyst having activity comparable to that of a Ru catalyst is of both scientific and practical importance.[14,15]

Transition metal nitrides have been gaining increasing attention because of their noble metal-like catalytic properties.[16] In ammonia synthesis and decomposition, however, nitrides are common species observed, especially in early transition-metal-containing catalysts. In the pioneering work of Mittasch, the nitrides of U, Mo, W, and Mn were found to form during ammonia synthesis.[17] Lotz et al. further investigated a number of 3d transition metal nitrides for ammonia decomposition and observed very limited activity at moderate temperatures.[18] Improved activity was found on a high-surface-area vanadium nitride at temperatures above 723 K.[19,20] Ternary nitrides containing elements from the right and left sides of the volcano curve and with optimal N binding energy,[21] such as Co–Mo–N and Ni–Mo–N, exhibit interesting performances in NH_3 decomposition.[21−24] More recently, the spongelike Fe_3N[25] and high-surface-area Mo-based nitrides[10,26,27] showing promises for NH_3 decomposition were reported.

Little investigation was given to Mn nitride as a catalyst for NH_3 decomposition because of its poor activity.[18] Recently, we demonstrated that lithium imide (Li_2NH) synergizes with Fe_2N, leading to unprecedentedly high catalytic activities in NH_3 decomposition through a two-step reaction path consisting of (I) $Li_2NH + Fe_2N \rightarrow Li_3FeN_2 + H_2$ and (II)

Received: February 9, 2015
Revised: March 16, 2015
Published: March 19, 2015

DOI: 10.1021/acscatal.5b00278
ACS Catal. 2015, 5, 2708−2713

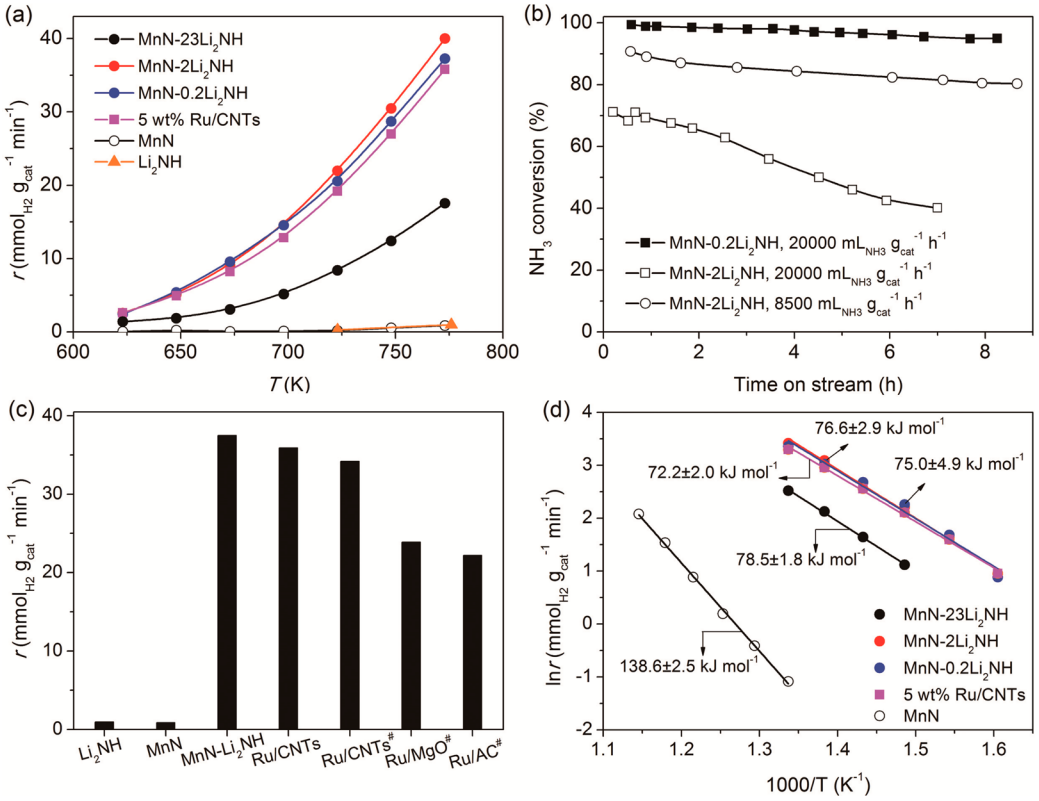

Figure 1. (a) Temperature dependence of the activities of Mn- and Ru-based catalysts on pure NH_3 decomposition. Reaction conditions: catalyst precursor loading, 30 mg; NH_3 flow rate, 30 mL min^{-1}. (b) Stability test of MnN−Li_2NH composite catalysts under different WHSVs. (c) Comparison of H_2 production rates over Li_2NH, MnN, MnN−Li_2NH catalyst and Ru-based catalysts at 773 K and WHSV = 60 000 mL_{NH_3} g_{cat}^{-1} h^{-1}. The activities of Ru/CNTs[#], Ru/MgO[#], and Ru/AC[#] are taken from reference 29. (d) Arrhenius plots of Mn- and Ru-based catalysts in the temperature range of 625−870 K and conditions described in part a, except MnN. E_a for MnN was determined under WHSV = 40 000 mL_{NH_3} g_{cat}^{-1} h^{-1} because of its low catalytic activity.

$Li_3FeN_2 + NH_3 \rightarrow Fe_2N + Li_2NH + N_2$. By extending the transition metal from Fe to other 3d elements, a universal and extraordinarily high catalytic activity was identified. Interestingly, the catalytic activities of 3d TM(N)−Li_2NH exhibit a unique volcano shape centered at the Mn site which is significantly different from the activity order of known catalysts.[21,28] In the present work, we aim to investigate the effect of catalyst composition on the catalytic performance as well as the reaction mechanism of the MnN−Li_2NH composite catalyst for NH_3 decomposition. Our experimental results reveal that a catalyst with high Mn content exhibits better stability. We also disclose the clear synergy between MnN and Li_2NH leading to a different reaction pathway, in which the more stable N-rich intermediate Li_7MnN_4 that tunes the energetics of the catalysis is formed. Kinetic analyses further disclose that the H_2 release step has a higher barrier than that of the N_2 release, in accordance with the relatively slow solid-state reaction between MnN and Li_2NH.

2. EXPERIMENTAL SECTION

2.1. Catalyst Preparation. Li_2NH was prepared by heating commercial $LiNH_2$ (Aldrich, 95.0%) at 773 K under vacuum for 24 h. MnN was prepared via the reaction between $MnCl_2$ (Alfa Aesar, 97%) and $LiNH_2$ with a molar ratio of 1:2. Typically, $LiNH_2$ (0.18 g) and $MnCl_2$ (0.5 g) were first ball-milled in an agate jar at 323 K (150 rpm for 3 h) on a Retsch planetary ball mill (PM 400), then the obtained black solid was heated to 773 K and held for 2 h in NH_3 flow (30 mL min^{-1}). The product was purified by stirring it in THF, followed by centrifugation three times to remove LiCl. The purified sample was then collected for use. The MnN−$x$$Li_2NH$ (x is the molar ratio of Li_2NH to MnN) composite catalysts were prepared via a procedure similar to that of MnN but with different $LiNH_2$/$MnCl_2$ molar ratios. Upon catalytic testing, the sample was heated to 573 K or above to allow $LiNH_2$ to decompose to Li_2NH. Li_7MnN_4 was prepared by heating a mixture of $MnCl_2$ and $LiNH_2$ with a molar ratio of 1:9 at 773 K for 2 h in Ar flow (30 mL min^{-1}). The obtained black powder was washed with THF several times to remove LiCl. The ammoniation of Li_7MnN_4 was performed in a homemade stainless steel reactor filled with pressurized NH_3. The gaseous product was analyzed by gas chromatography, and the solid products were characterized by XRD. Because Li metal, $LiNH_2$, and self-made Mn-based samples are sensitive to moisture and oxygen, all the samples were stored and handled in a glovebox filled with Ar.

2.2. Catalyst Characterization. XRD patterns were recorded on a PANalytical X'pert diffractometer using a homemade sample cell covered with KAPTON film to avoid air or moisture contamination. Temperature-programmed decomposition (TPD) measurements were performed in a tubular quartz reactor, and the effluent gases were analyzed by a mass spectrometer (Hiden HPR20). Samples were heated in Ar flow (30 mL min^{-1}) from room temperature to the desired temperatures at prefixed ramping rates.

DOI: 10.1021/acscatal.5b00278
ACS Catal. 2015, 5, 2708−2713

2.3. Catalyst Test. Ammonia decomposition was performed in a continuous-flow, fixed-bed, quartz reactor (i.d. = 4 mm) at ambient pressure. Typically, 30 mg of catalyst or its precursor was loaded, and the temperature was raised at a ramping rate of 5 K min^{-1}. The effluent gases were analyzed using an online gas chromatograph (GC-2014C, Shimadzu) equipped with Porapak N and 5A molecular sieve columns and a thermal conductivity detector. Ammonia conversion data reported here were collected after 30 min on-stream at the corresponding temperature.

3. RESULTS AND DISCUSSION

Li_2NH or MnN shows little catalytic activity below 750 K under the reaction conditions applied here (Figure 1a). The addition of a small amount of Mn to Li_2NH (molar ratio of Mn to Li_2NH is 1:23, denoted as MnN−23Li_2NH) leads to an observable activity at a temperature as low as 623 K, which was achieved only by Ru-based catalysts.[29] Upon increasing the Mn content (MnN−2Li_2NH), the NH_3 conversion rate doubles in the temperature range of 650−773 K. The stability of the MnN−Li_2NH catalyst was monitored under pure NH_3 at 823 K. As shown in Figure 1b, a relatively quick activity loss from ∼70% to 40% of NH_3 conversion degree was found on the MnN−2Li_2NH catalyst during a testing period of 7 h at WHSV (weight hourly space velocity) = 20 000 mL_{NH_3} g_{cat}^{-1} h^{-1}, whereas at a lower WHSV (8500 mL_{NH_3} g_{cat}^{-1} h^{-1}), a relatively slower activity loss from ∼90% to 80% was observed during a period of 8 h. The activity loss may be ascribed to the formation (via R1), melting (mp 650 K), and loss of $LiNH_2$ under the reaction condition.

$$Li_2NH + NH_3 = 2LiNH_2 \quad (R1)$$

Li_2NH reacts with NH_3 forming $LiNH_2$ according to reaction R1. Under high temperatures or low NH_3 pressures, such a reaction is not thermodynamically favored. In the NH_3 decomposition reaction, the increase in NH_3 conversion degree (i.e., under lower WHSV) will reduce the chance of formation of $LiNH_2$. Therefore, the changes in catalyst composition and textural structure (i.e., specific surface area, particle size, etc.) caused by the melting and loss of $LiNH_2$ may not be significant, and a relatively stable performance of the catalyst can be achieved. Under higher WHSV when NH_3 partial pressure is higher, the formation of $LiNH_2$ is favored, and consequently, the losses of $LiNH_2$ from the catalyst and its corresponding activity would be severe, which is evidenced by a substantial catalyst weight loss (i.e., from 30 to 22 mg) and activity drop within a relatively short reaction time (Figure 1b). Under a diluted NH_3 flow (5 vol % NH_3/Ar), where the chance of $LiNH_2$ formation is even less, essentially no observable activity drop for the MnN−2Li_2NH sample within a testing period of 12 h at 723 K (Figure S1) resulted. Such an experimental result further supports our hypothesis on the cause of activity loss.

This finding reveals that Li_2NH is not a rigid matter maintaining the structural stability of the catalyst. We thus worked on catalysts with a high Mn content. As shown in Figure 1a, the MnN−0.2Li_2NH has an activity nearly identical to that of MnN−2Li_2NH and achieves an unprecedented H_2 production rate of 37.5 mmol g_{cat}^{-1} min^{-1} at 773 K, which is superior to the highly active 5 wt % Ru/CNTs synthesized by us and reported in reference 29, ∼40 times that of MnN and Li_2NH, and over 1.5 times as much as the data reported in the Ru/MgO and Ru/AC catalysts[29] (see Figure 1c). It is noteworthy that NH_3 conversion can be retained at ∼90% during a testing period of 8 h at 823 K and WHSV = 20 000 mL_{NH_3} g_{cat}^{-1} h^{-1} over the MnN−0.2Li_2NH (Figure 1b). On the basis of the observations described above, we would like to propose three ways to alleviate the activity drop of the MnN−Li_2NH composite system. First, choose the proper reaction conditions to achieve a high NH_3 conversion degree to reduce the possibility of the formation of $LiNH_2$. Second, add suitable substances that can stabilize $LiNH_2$. Third, employ a suitable reactor (such as a U-shaped or tank reactor[15,28]), which can retain $LiNH_2$ within the vicinity of the MnN. Further optimization is needed.

Figure 1d shows the Arrhenius plots of the Mn- and Ru-based catalysts. The apparent activation energy for MnN is 138.6 ± 2.5 kJ mol^{-1}, which is consistent with the value reported by Lotz et al.[18] The apparent activation energies for MnN−2Li_2NH and MnN−0.2Li_2NH catalysts (76.6 ± 2.9 and 75.0 ± 4.9 kJ mol^{-1}, respectively) are much smaller than that of MnN and close to that of Ru/CNTs (72.2 ± 2.0 kJ mol^{-1}).[29] The similar apparent activation energies of MnN−Li_2NH and Ru indicate that the MnN−Li_2NH has the potential to compare with Ru within a wide range of reaction temperatures. The significant decrease in apparent activation energies of the MnN−Li_2NH catalysts also indicates a change in the reaction pathway from that of MnN, which will be discussed later.

NH_3 decomposition over transition metals or metal nitrides proceeds through successive dehydrogenation and follow-up recombinative desorption of adsorbed N and H atoms. Previous kinetic studies indicate that at low temperatures, the recombinative desorption of adsorbed N atoms is the rate-determining step (RDS).[30] For a transition metal surface precovered by nitrogen (such as FeN_x, $0 < x \leq 1$), on the other hand, the rate of dehydrogenation of NH_x (x = 1, 2, 3) was proposed to be slow as a result of insufficient coordination of intermediate NH_y (y = 0, 1, 2) by the transition metal.[31] It is, therefore, understandable that under higher NH_3 partial pressure where MnN is the stable phase, the catalytic activity is poor, as evidenced by the experimental results shown in Figure 1a. It is expected that upon removing N from the MnN surface to free some of the Mn sites, NH_3 decomposition could find a place to occur. This hypothesis is strongly supported by the experimental facts that under lower NH_3 partial pressure (5 vol % NH_3), an appropriate activity of the MnN sample can be observed at 673 K and above (Figure S2a), which is nicely consistent with the occurrence of the decomposition of MnN (Figure S2b). Similarly, the presence of a MoN_x phase ($x < 1$, depending on the temperature) rather than MoN was also observed in situ by XRD when NH_3 decomposition took place at an appropriate rate.[27]

The drastically increased activity and reduced kinetic barrier of the MnN−Li_2NH composite catalyst manifest the changes in the reaction pathway. The MnN−2Li_2NH sample collected after the decomposition of pure NH_3 at 723 K followed by quick cooling to room temperature in NH_3 flow contains Li_2NH and MnN phases (Figure 2a). Note that neither Li_2NH nor MnN shows appropriate activity below 750 K (Figure 1a), and a synergy between the two components should take place to account for the abnormally high catalytic performance.

The TPD-MS measurement (Figure S3) shows that Li_2NH can react with MnN above 550 K to release H_2, NH_3, and minor N_2 (N_2 and part of the H_2 may come from the decomposition of NH_3 over the catalyst under the conditions

DOI: 10.1021/acscatal.5b00278
ACS Catal. 2015, 5, 2708−2713

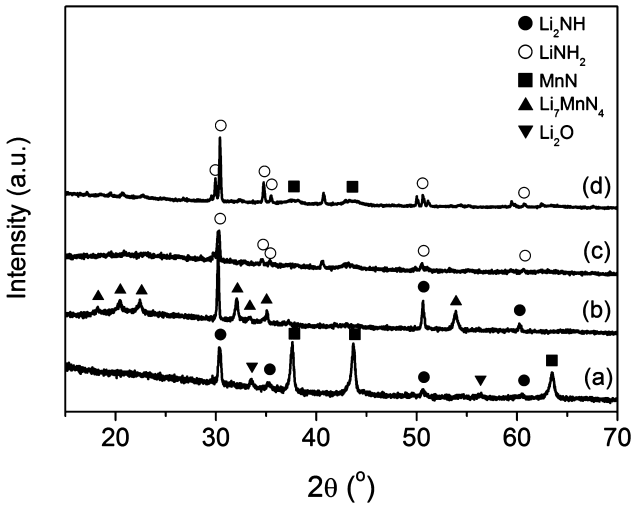

Figure 2. XRD patterns for the MnN−2Li_2NH sample collected after testing at 723 K (a), the MnN−2Li_2NH after TPD (b), Li_7MnN_4 after ammoniation at ambient temperature (c), and heated at 473 K for 3 h (d).

applied). The XRD characterization of the post-TPD solid residue evidence the formation of Li_7MnN_4 (Figure 2b), supporting the occurrence of R2. Li_7MnN_4, on the other hand, can be easily ammoniated to release N_2 (Figure 3a) and form a solid mixture of $LiNH_2$ and an amorphous Mn-containing mixture at room temperature (Figure 2c). Heating this solid mixture at 473 K in an Ar flow results in the presence of crystalline $LiNH_2$ and MnN (Figure 2d). At temperatures above 523 K, the decomposition of $LiNH_2$ to Li_2NH takes place. The overall process can be seen in eq R3. The net reaction is R4, that is, NH_3 decomposes to N_2 and H_2.

$$(7/2)Li_2NH + MnN = Li_7MnN_4 + H_2 + (1/2)NH_3 \quad (R2)$$

$$Li_7MnN_4 + (7/6)NH_3 = (7/2)Li_2NH + MnN + (1/6)N_2 \quad (R3)$$

$$NH_3 = (1/2)N_2 + (3/2)H_2 \quad (R4)$$

It is worth noting that if the Li_7MnN_4 sample was heated in NH_3 flow to 625 K or above, catalytic activity was observed (Figure S4a). The active phases were found to be MnN and Li_2NH (Figure S4b).

Although there may be other paths accounting for the catalytic process, the facile occurrences of R2 and R3 at moderate temperatures suggest that they are likely the main course for the catalysis, which is also supported by the thermodynamic calculations (shown in Figure S5). Both reactions have a chance to take place in the temperature range of 600−800 K, in agreement with the experimental observation, that is, catalytic activity is observable at 623 K (Figure 1a). Comparatively, the presence of Li_2NH and MnN is favored under higher NH_3 partial pressure or relatively lower temperatures; under low NH_3 partial pressure or at elevated temperatures (or both), Li_7MnN_4 is the main phase, in excellent agreement with the experimental finding (indeed, the coexistence of Li_2NH, MnN, and Li_7MnN_4 was observed on a sample collected upon catalyzing NH_3 decomposition at 773 K under 5 vol % NH_3, see Figure S6).

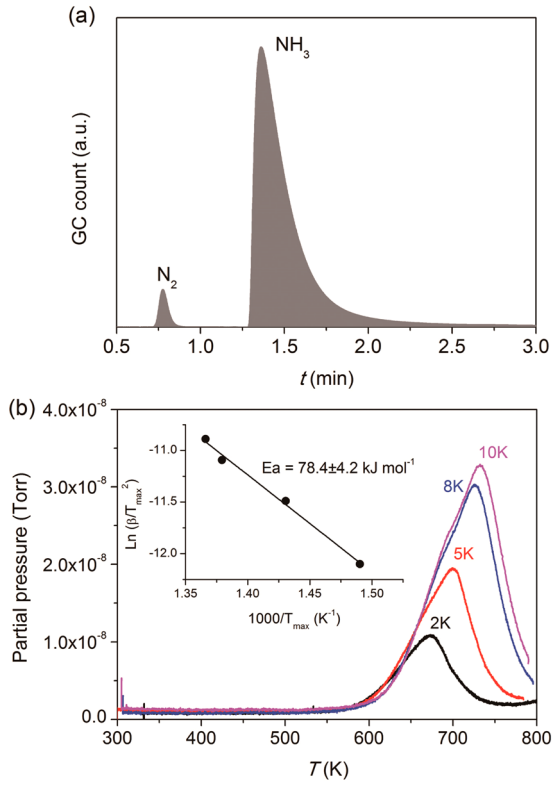

Figure 3. (a) GC evidence of N_2 formation after ammoniation of Li_7MnN_4 at ambient temperature. (b) H_2−TPD profiles of the MnN−12Li_2NH sample, which was prepared by ball-milling the two components for 2 h. The ramping rates, β, employed here are 2, 5, 8, and 10 K min^{-1}. The inset is the Kissinger's plot. The activation energy of H_2 release is 78.4 ± 4.2 kJ mol^{-1}, calculated by using the Kissinger equation, namely, $\ln(\beta/T_{max}^2) = \ln(AR/E_a) - E_a/RT_{max}$. T_{max} is the peak temperature of the H_2−TPD profile, A is the pre-exponential factor, and R is the gas constant.

Alkalis have been widely employed as electronic promoters in a variety of heterogeneous catalysts.[32] It has been proposed that alkali would affect the local electronic structure of active metals probably by electron donation or electrostatic interactions in catalytic NH_3 synthesis and decomposition.[1,33,34] The promoting capability has been found to be in the order of Cs > K > Na > Li,[1,35] among which Li is commonly regarded as the least promoting one and, hence, receives little attention. In this specific catalytic system, however, Li_2NH enhances the catalytic activity of MnN significantly, and more interestingly, it plays a different role.[28] As inferred from the R2 and R3, it is on one hand the NH_3 transmitting agent having an activated N−H bonding (IR: N−H stretch at 3160 cm^{-1} in Li_2NH vs 3340 cm^{-1} in NH_3) and repeatedly consumed and regenerated through the R1 and R2; on the other hand, it reacts with MnN, leading to the formation of the ternary nitride with unusually high N content, that is, Li_7MnN_4 is equivalent to (7/3)Li_3N + (1/3)Mn_3N_5. Note that such a high N content (Mn_3N_5) is inaccessible by binary manganese nitride. For instance, MnN is reported to be the thermodynamically stable form of the highest N content, in which the molar ratio of Mn to N is ~1:1.[36]

The retention of a high N content by Mn in Li_7MnN_4 should be ascribed to the presence of Li. Li, as other alkalis or alkaline earths that can form stable transition metal oxides, nitrides, and oxynitrides in unusually high oxidation states, executes a

DOI: 10.1021/acscatal.5b00278
ACS Catal. 2015, 5, 2708−2713

positive inductive effect,[37−39] increasing the overlap between the d orbitals of Mn and the destabilized N 2p state[40] and, thus, strengthens the covalent Mn−N bonding, stabilizing the Li_7MnN_4 structure. Moreover, the highly mobile Li^+ and H^+ in Li_2NH[41,42] facilitate the occurrence of the solid-state reaction, R2, leading to the detectable Li_7MnN_4 phase. Li_2NH can be regarded as a H store playing an oxidizing role converting MnN to Li_7MnN_4 (a N store); part of H is reduced to H_2, the other part of H may migrate toward N nearby, forming NH_3. The N store, Li_7MnN_4, on the other hand, can be easily reduced by NH_3, giving off N_2. We suppose that Li^+ in Li_7MnN_4 executes an attraction to adsorb NH_3, and thus, the interaction between Li^+ and the $[MnN_4]^{7-}$ is weakened. The reduced inductive effect of Li^+ on the covalent Mn−N bonding will lead the unstable $[MnN_4]$ motif to collapse via the redox reaction between Mn^{5+} and N^{3-} to form N_2 and MnN.

The substantial reduction of E_a from 139 (MnN) to ∼75 kJ mol^{-1} in the presence of Li_2NH reveals that the energy barriers for desorption of N_2 and dehydrogenation of NH_x should be lowered. Moreover, the relatively higher onset temperature for H_2 release from MnN−Li_2NH (above 550 K; see Figure 3b) as compared with the H_2 desorption temperature from the surfaces of Ru, Fe, Ni, and Co,[43−47] suggests that the H_2 release step may be kinetically slow in the MnN−Li_2NH system. To support this hypothesis, the kinetics of H_2 release (R2) and N_2 release (R3) steps were investigated. Figure 3b show the H_2−TPD profiles of the MnN−Li_2NH sample with different ramping rates (β = 2, 5, 8, and 10 K min^{-1}). By employing Kissinger's method,[48] the slope of the plot of $\ln(\beta/T_{max}^2)$ as a function of $1/T_{max}$ (shown in Figure 3b) can give the activation energy for H_2 release, which is 78.4 ± 4.2 kJ mol^{-1}. The similar E_a for H_2 release and for the overall NH_3 decomposition (∼75 kJ mol^{-1}) implies that the H_2 release should be kinetically significant. In contrast, the ammoniation of Li_7MnN_4 can be easily carried out at ambient temperature with the formation of N_2, which manifests that it is unlikely to be rate-limiting, especially in the temperature range applied (623−823 K). Under this scenario, a relatively weak influence of NH_3 partial pressure on the reaction rate is expected. The reaction order, α, with regard to NH_3 in the power law equation of $r = kP_{NH_3}^{\alpha}$ was measured at 623 and 648 K, respectively (Figure 4). The straight fitted lines give a fairly low value of 0.2, further supporting that R3 is not likely involved in the rate-limiting step for the MnN−Li_2NH system.

It should be noted that the above-mentioned two reactions, R2 and R3, may not be elementary steps. The details of each reaction remain subjects of surface science characterization and theoretical modeling. In view of the key role of Li_2NH in this unique MnN−Li_2NH catalytic system, the long pursued issue of electronic promotion by alkalis may be revisited. The understanding on the roles of alkalis in heterogeneous catalysis will benefit the design and development of more active and less expensive catalyst for chemical and energy productions. With the powerfulness of the high-throughput calculation, such a pace would be faster leading to an enriched understanding on catalysis and broadened materials scope for catalysts.

4. CONCLUSIONS

In summary, we demonstrate that MnN, which is essentially inactive for ammonia decomposition, can function as a highly active catalyst, surpassing Ru when synergizing with Li_2NH. A hydrogen production rate of 37.5 mmol g_{cat}^{-1} min^{-1}, which is 40-fold that of MnN, over 1.5 times as much as that of the Ru/MgO and Ru/AC, and even superior to the highly active 5 wt % Ru/CNTs at 773 K, can be achieved under the same reaction conditions. The MnN-rich catalyst shows better stability compared with the Li_2NH-rich catalyst. The apparent activation energy of MnN−Li_2NH is similar to that of the Ru/CNTs catalyst, which implies its potential to replace noble metals for NH_3 decomposition. A two-step catalytic cycle accounting for the synergistic effect between Li_2NH and MnN has been identified. The desorption of N_2, which is the RDS in the conventional transition metal or nitride catalyzation process, appears to be fast for the MnN−Li_2NH catalyst. H_2 release, in contrast, is kinetically slow.

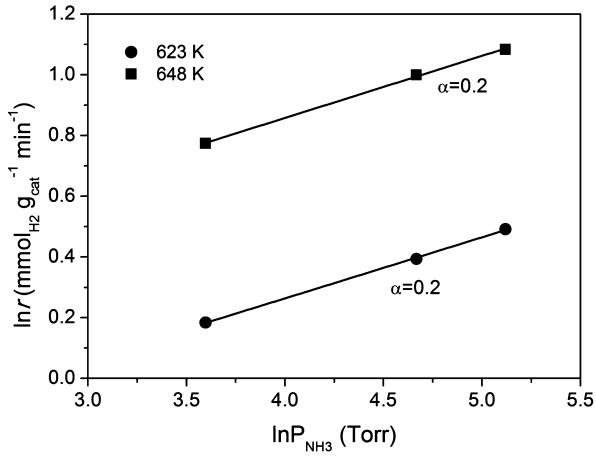

Figure 4. Reaction orders of NH_3 over MnN−0.2Li_2NH at 623 and 648 K, respectively. The partial pressure of NH_3 was varied from 5 to 22 vol % with a constant total pressure of 1 bar.

■ ASSOCIATED CONTENT

Supporting Information

The following file is available free of charge on the ACS Publications website at DOI: 10.1021/acscatal.5b00278.

Catalytic activities and TPD profiles of Mn-based catalysts, XRD patterns of spent Mn-based catalysts, thermodynamic estimations (PDF)

■ AUTHOR INFORMATION

Corresponding Author

*E-mail: pchen@dicp.ac.cn.

Present Address

∥(D.H.) School of Science, University of Science and Technology Liaoning, Anshan 114051, People's Republic of China.

Notes

The authors declare no competing financial interest.

■ ACKNOWLEDGMENTS

This work was supported by the Project of National Natural Science Funds for Distinguished Young Scholars (51225206), and 973 Project (2010CB631304), People's Republic of China.

■ REFERENCES

(1) Yin, S. F.; Xu, B. Q.; Zhou, X. P.; Au, C. T. *Appl. Catal., A* **2004**, *277*, 1−9.

(2) Klerke, A.; Christensen, C. H.; Nørskov, J. K.; Vegge, T. *J. Mater. Chem.* **2008**, *18*, 2304−2310.

DOI: 10.1021/acscatal.5b00278
ACS Catal. 2015, 5, 2708−2713

(3) Schüth, F.; Palkovits, R.; Schlögl, R.; Su, D. S. *Energy Environ. Sci.* **2012**, *5*, 6278−6289.
(4) Ji, J.; Duan, X. Z.; Qian, G.; Zhou, X. G.; Chen, D.; Yuan, W. K. *Ind. Eng. Chem. Res.* **2013**, *52*, 1854−1858.
(5) García-Bordejé, E.; Armenise, S.; Roldán, L. *Catal. Rev. Sci. Eng.* **2014**, *56*, 220−237.
(6) Armenise, S.; Roldán, L.; Marco, Y.; Monzon, A.; García-Bordejé, E. *J. Phys. Chem. C* **2012**, *116*, 26385−26395.
(7) Lu, A. H.; Nitz, J. J.; Comotti, M.; Weidenthaler, C.; Schlichte, K.; Lehmann, C. W.; Terasaki, O.; Schüth, F. *J. Am. Chem. Soc.* **2010**, *132*, 14152−14162.
(8) Zhang, J.; Muller, J. O.; Zheng, W. Q.; Wang, D.; Su, D. S.; Schlögl, R. *Nano Lett.* **2008**, *8*, 2738−2743.
(9) Simonsen, S. B.; Chakraborty, D.; Chorkendorff, I.; Dahl, S. *Appl. Catal., A* **2012**, *447*, 22−31.
(10) Zheng, W. Q.; Cotter, T. P.; Kaghazchi, P.; Jacob, T.; Frank, B.; Schlichte, K.; Zhang, W.; Su, D. S.; Schüth, F.; Schlögl, R. *J. Am. Chem. Soc.* **2013**, *135*, 3458−3464.
(11) Pelka, R.; Kielbasa, K.; Arabczyk, W. *J. Phys. Chem. C* **2014**, *118*, 6178−6185.
(12) Li, L.; Zhu, Z. H.; Yan, Z. F.; Lu, G. Q.; Rintoul, L. *Appl. Catal., A* **2007**, *320*, 166−172.
(13) Hayashi, F.; Toda, Y.; Kanie, Y.; Kitano, M.; Inoue, Y.; Yokoyama, T.; Hara, M.; Hosono, H. *Chem. Sci.* **2013**, *4*, 3124−3130.
(14) Hansgen, D. A.; Vlachos, D. G.; Chen, J. G. G. *Nat. Chem.* **2010**, *2*, 484−489.
(15) David, W. I. F.; Makepeace, J. W.; Callear, S. K.; Hunter, H. M. A.; Taylor, J. D.; Wood, T. J.; Jones, M. O. *J. Am. Chem. Soc.* **2014**, *136*, 13082−13085.
(16) Hargreaves, J. S. J. *Coord. Chem. Rev.* **2013**, *257*, 2015−2031.
(17) Mittasch, A.; Frankenburg, W. *Adv. Catal.* **1950**, *2*, 81−104.
(18) Lotz, C. R.; Sebba, F. *Trans. Faraday Soc.* **1957**, *53*, 1246−1252.
(19) Oyama, S. T. *J. Catal.* **1992**, *133*, 358−369.
(20) Choi, J. G.; Jung, M. K.; Choi, S.; Park, T. K.; Kuk, I. H.; Yoo, J. H.; Park, H. S.; Lee, H. S.; Ahn, D. H.; Chung, H. S. *Bull. Chem. Soc. Jpn.* **1997**, *70*, 993−996.
(21) Boisen, A.; Dahl, S.; Nørskov, J. K.; Christensen, C. H. *J. Catal.* **2005**, *230*, 309−312.
(22) Liang, C. H.; Li, W. Z.; Wei, Z. B.; Xin, Q.; Li, C. *Ind. Eng. Chem. Res.* **2000**, *39*, 3694−3697.
(23) Duan, X. Z.; Qian, G.; Zhou, X. G.; Chen, D.; Yuan, W. K. *Chem. Eng. J.* **2012**, *207*, 103−108.
(24) Ji, J.; Duan, X. Z.; Qian, G.; Zhou, X. G.; Tong, G. S.; Yuan, W. K. *Int. J. Hydrogen Energy* **2014**, *39*, 12490−12498.
(25) Schnepp, Z.; Thomas, M.; Glatzel, S.; Schlichte, K.; Palkovits, R.; Giordano, C. *J. Mater. Chem.* **2011**, *21*, 17760−17764.
(26) Tagliazucca, V.; Schlichte, K.; Schüth, F.; Weidenthaler, C. *J. Catal.* **2013**, *305*, 277−289.
(27) Tagliazucca, V.; Leoni, M.; Weidenthaler, C. *Phys. Chem. Chem. Phys.* **2014**, *16*, 6182−6188.
(28) Guo, J. P.; Wang, P. K.; Wu, G. T.; Wu, A. A.; Hu, D. Q.; Xiong, Z. T.; Wang, J. H.; Yu, P.; Chang, F.; Chen, Z.; Chen, P. *Angew. Chem., Int. Ed.* **2015**, *54*, 2950−2954.
(29) Yin, S. F.; Xu, B. Q.; Ng, C. F.; Au, C. T. *Appl. Catal., B* **2004**, *48*, 237−241.
(30) Chellappa, A. S.; Fischer, C. M.; Thomson, W. J. *Appl. Catal., A* **2002**, *227*, 231−240.
(31) Yeo, S. C.; Han, S. S.; Lee, H. M. *J. Phys. Chem. C* **2014**, *118*, 5309−5316.
(32) Koel, B. E.; Kim, J. Promoters and Poisons. In *Handbook of Heterogeneous Catalysis*; Ertl, G., Knözinger, H., Schüth, F., Weitkamp, J., Eds.; Wiley-VCH: Weinheim, 2008; Vol. 3, pp 1593−1624.
(33) Dahl, S.; Logadottir, A.; Jacobsen, C. J. H.; Nørskov, J. K. *Appl. Catal., A* **2001**, *222*, 19−29.
(34) de Smit, E.; Weckhuysen, B. M. *Chem. Soc. Rev.* **2008**, *37*, 2758−2781.
(35) Aika, K.; Takano, T.; Murata, S. *J. Catal.* **1992**, *136*, 126−140.
(36) Suzuki, K.; Kaneko, T.; Yoshida, H.; Obi, Y.; Fujimori, H.; Morita, H. *J. Alloys Compd.* **2000**, *306*, 66−71.
(37) Etourneau, J.; Portier, J.; Menil, F. *J. Alloys Compd.* **1992**, *188*, 1−7.
(38) Tapia-Ruiz, N.; Segales, M.; Gregory, D. H. *Coord. Chem. Rev.* **2013**, *257*, 1978−2014.
(39) Wu, Y. B.; Lazic, P.; Hautier, G.; Persson, K.; Ceder, G. *Energy Environ. Sci.* **2013**, *6*, 157−168.
(40) Kurzman, J. A.; Misch, L. M.; Seshadri, R. *Dalton Trans.* **2013**, *42*, 14653−14667.
(41) David, W. I. F.; Jones, M. O.; Gregory, D. H.; Jewell, C. M.; Johnson, S. R.; Walton, A.; Edwards, P. P. *J. Am. Chem. Soc.* **2007**, *129*, 1594−1601.
(42) Miceli, G.; Cucinotta, C. S.; Bernasconi, M.; Parrinello, M. *J. Phys. Chem. C* **2010**, *114*, 15174−15183.
(43) Shi, H.; Geng, P.; Jacobi, K. *Surf. Sci.* **1994**, *315*, 1−8.
(44) Grunze, M.; Bozso, F.; Ertl, G.; Weiss, M. *Appl. Surf. Sci.* **1978**, *1*, 241−265.
(45) Ertl, G.; Lee, S. B.; Weiss, M. *Surf. Sci.* **1981**, *111*, L711−L715.
(46) Vlachos, D. S.; Papageorgopoulos, C. A. *Appl. Surf. Sci.* **1998**, *136*, 230−237.
(47) van Helden, P.; van den Berg, J. A.; Weststrate, C. J. *ACS Catal.* **2012**, *2*, 1097−1107.
(48) Kissinger, H. E. *Anal. Chem.* **1957**, *29*, 1702−1706.

DOI: 10.1021/acscatal.5b00278
ACS Catal. 2015, 5, 2708−2713